ADVANCED ELECTRONIC MATERIALS
www.advelectronicmat.de

Ultra-Wideband Integrated Graphene-Based Absorbers for Terahertz Waveguide Systems

*James Campion, Nikolaos Xenidis, Serguei Smirnov, Roman Ivanov, Joachim Oberhammer, Irina Hussainova, and Dmitri Lioubtchenko**

This article presents novel graphene-based absorber materials which can be directly integrated in terahertz waveguide systems. A simple, low-cost integration method is developed, allowing graphene augmented inorganic nanofibers to be embedded inside a metallic waveguide. In contrast to existing absorbers, the ability to embed such materials in a metallic waveguide allows them to be integrated into complete terahertz systems for large-scale applications. The electromagnetic properties of such materials are then examined using standard network analysis techniques. A wideband measurement setup is developed to enable measurement of a single sample from 67 to 500 GHz, eliminating the need to fabricate multiple samples. The porosity of the integrated material leads to excellent electromagnetic performance across a wide range of frequencies. The samples are found to have a reflection coefficient less than −10 dB for frequencies above 200 GHz, while their attenuation per unit length exceeds 35 dB mm^{-1}. The low reflectivity of the material allows it to be used in systems applications where undesired reflections must be avoided. The electromagnetic shielding effectiveness of the material is assessed, with a total effectiveness of 20–45 dB observed for 0.84 mm thick samples.

1. Introduction

Historically, terahertz science and technology has been restricted to specialized applications such as radio astronomy due to various technological challenges.[1] This scenario is set to change, however, due to the rapid development of integrated electronic and photonic components for terahertz applications over the past 2 decades.[2,3] The terahertz spectrum (0.1–10 THz) is of great interest to both the academic and industrial sectors due to the unique properties of the spectrum and of terahertz radiation. This spectrum will form the backbone of the next generation of wireless technology, 6G, where the wide swathes of available bandwidth will enable new solutions that can revolutionize everyday life.[4–6] Aside from wireless communications, the industrial applications of terahertz technology include sensing and imaging,[7,8] spectroscopy[9] and radar.[10,11] Deploying such systems will create an unprecedented demand for materials that can absorb terahertz radiation, to limit unwanted interference and provide effective electromagnetic shielding.[12,13] The diversity of these applications, as well as their large-scale nature, will require absorber materials that are low-cost, compact, insensitive to environmental conditions and which can be directly integrated into the system in question. As such, the availability of effective absorbing materials is one of the key enablers for the realization of complete terahertz systems.

Hollow rectangular waveguides are the primary transmission line medium in many terahertz systems due to their mechanical stability, low electromagnetic losses, enclosed nature, and their compatibility with active circuit elements.[14,15] Electromagnetic wave devices such as circulators, couplers, and power dividers require that one or more of their ports be terminated to eliminate unwanted signals and ensure correct operation. Waveguide terminations are often realized by short-circuited waveguide sections which present low reflection and absorb the incident energy due to the presence of an absorbing material inside the waveguide.[16] An ideal waveguide termination should have low reflectivity across a wide band of frequencies and be stable across a range of operating temperatures and environmental conditions.[17] Achieving low reflectivity in a termination requires that the incident energy be transmitted

J. Campion, N. Xenidis, S. Smirnov, J. Oberhammer, D. Lioubtchenko
Division of Micro and Nanosystems
KTH Royal Institute of Technology
Stockholm 100 44, Sweden
E-mail: dml@kth.se

R. Ivanov, I. Hussainova
Department of Mechanical and Electrical Engineering
Tallinn University of Technology
Tallinn 19086, Estonia

J. Campion
TeraSi AB
Stockholm 139 33, Sweden

D. Lioubtchenko
CENTERA Laboratories
Institute of High-Pressure Physics PAS
Warsaw 01-142, Poland

The ORCID identification number(s) for the author(s) of this article can be found under https://doi.org/10.1002/aelm.202200106.

DOI: 10.1002/aelm.202200106

through the material's interface and undergo sufficient attenuation within the material such that the signal reflected by the short-circuit is entirely absorbed. This places contradicting requirements on the absorber material, which should both be of a similar impedance to the waveguide while offering high absorbance. Conventional microwave terminations typically use magnetic absorbers which are machined or molded to the desired form, a process that is easily performed at microwave frequencies. Tapering is applied as a means of reducing the step change in impedance at the material's interface, improving bandwidth and reflectivity.[16] Free-space absorbers frequently consist of a porous material which is loaded with lossy particles and are also commonly tapered. Carbon and ferrite-carbon composite based absorbers of this type[18] find widespread use in anechoic chambers.[19] However, the required tapering results in long absorbers of complex geometry, limiting their potential integration. At higher frequencies, such as in the terahertz spectrum, these tapers become extremely challenging to realize. For successful system integration an absorber must be compatible with semiconductor processing techniques, which typically require temperature treatment at 300–500 °C. This prohibits the use of epoxy or polymer-based solutions. Periodic structures or metamaterials may be employed as an alternative means of realizing absorbers and can even allow for tuning of the absorption properties.[20–24] The operational bandwidth of such devices is limited by their inherent periodicity, while their implementation requires precision fabrication.[21]

The aforementioned requirements and the limitations of existing solutions drive the search for new absorber materials, where a variety of approaches have been reported to date. Epoxy composites are efficient absorbers and electrical insulators.[25,26] However, due to differences in their coefficient of thermal expansion, these rigid materials can crack or flake when placed in a waveguide. Due to the mirror-like surfaces formed during curing, low reflection coefficients are difficult to achieve with epoxy based composites. The ongoing development of new nanomaterials, both porous[27] and fiber-like,[28] offers new alternatives to traditional microwave absorber materials. Among these, carbon-based materials are the most promising, as documented in many studies to date.[29,30] These materials effectively absorb electromagnetic waves due to the presence of sp^2 carbon.[18] The use of nanomaterials provides additional benefits over their traditional counterparts. Low density foams and aerogels reduce component weight and allow for improved control of the absorber's electromagnetic properties,[31] as the introduction of air reduces its effective permittivity. This reduces the impedance mismatch which occurs at the interface between air and the absorber, improving its return loss and operational bandwidth. Materials based on carbon nanotubes (CNTs) are of great interest due to their effective electromagnetic absorption properties and ability to withstand up to 1000 °C without destruction,[32] enabling their use in standard CMOS and MEMS processing. CNTs can be formed in a bubble-like structure that can provide electromagnetic wave absorption with low reflections provided that the features are electrically large at the frequency of operation. The bubble-like structure of CNTs in a polymer matrix has successfully been used to form a CNT-based absorber, with good performance for a frequency range of 8–16 GHz,[33] 5-40 GHz,[34] and 75–110 GHz.[35] The performance of such materials above 110 GHz has not been reported to date. In addition, these materials may necessitate additional chemical treatments to improve their performance,[35] adding fabrication cost and complexity. Graphene-based materials are also promising candidates for terahertz absorbers, as they offer extremely wide absorption bandwidths and absorbance levels.[36–38] Graphene aerogels can be realized using freeze-drying techniques[39] and have been utilized as tunable terahertz absorbers,[12] where an external bias voltage or pump laser is applied to modulate the conductivity of the embedded graphene layers. The performance of similar graphene aerogels at microwave frequencies was evaluated in ref. [40], where they were found to offer excellent absorption across a narrow band of frequencies. However, none of the previously reported graphene-based absorbers have been successfully integrated into a rectangular waveguide suitable for use at terahertz frequencies, preventing their use in complete systems. Many previously reported absorbers also require the use of layered structures and lithography techniques, limiting their scalability due to the associated increase in fabrication cost.

Here, we present a new kind of ultra-wideband THz absorber which is directly integrated in a standard metallic waveguide, allowing it to be used in conventional THz systems and applications. The absorber material is comprised of graphene-augmented inorganic nanofibers (GAIN) which are deposited in a rectangular waveguide cassette using standard processing techniques. This cassette is then inserted in a specialized holder to allow it to be integrated in a waveguide system for characterization. The electromagnetic properties of the material are analyzed from 67 to 500 GHz, while the morphology and constitution of the material is examined using scanning electron microscopy, X-ray photoelectron, and Raman spectroscopy. The integration method developed here is easily scalable to different frequency ranges and waveguide geometries and requires only standard laboratory equipment and techniques, making it viable for high-volume production.

2. Results and Discussion

The novel integrated absorber reported in this work is illustrated in **Figure 1**, wherein a GAIN solid is heterogeneously integrated in the body of a metallic waveguide cassette. This cassette is designed such that it can be directly inserted in conventional terahertz waveguide systems, overcoming the limitations of many of the previously reported absorber materials. The waveguide aperture in the cassette is filled with a GAIN solid which acts as an integrated terahertz absorber. The GAIN

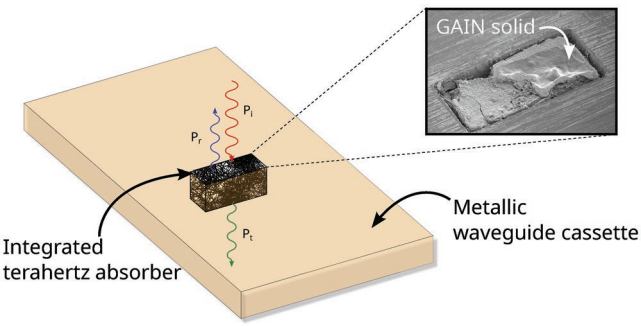

Figure 1. Illustration of the integrated terahertz absorber developed here.

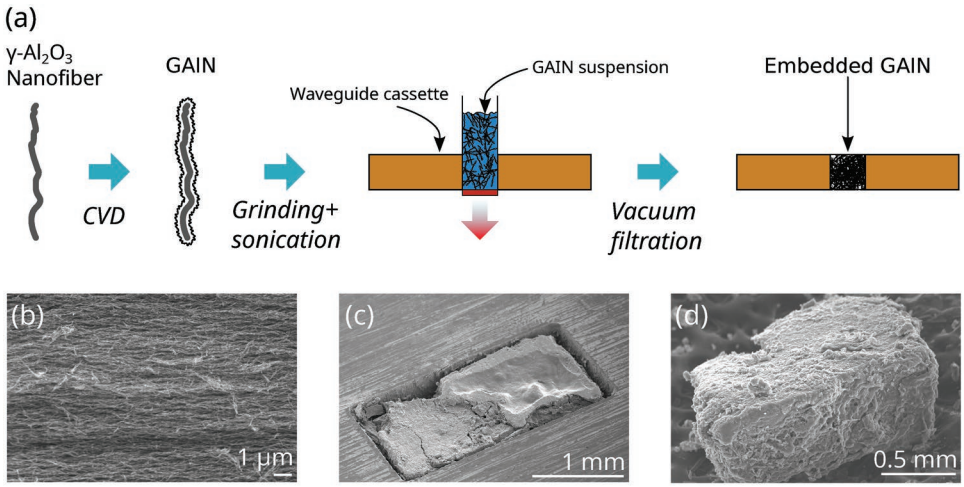

Figure 2. a) Illustration of the proposed waveguide integration method. b-d) SEM images of GAIN sample prior to grinding and sonication (b), a waveguide cassette with integrated GAIN (c), and an integrated GAIN sample which has subsequently been removed from the waveguide (d).

solid is comprised of a tightly-bound network of randomly distributed GAIN fibers and is directly embedded in the cassette via a simple three-step process (**Figure 2**a). GAIN is first realized from γ-Al_2O_3 nanofibers following.[28] The carbon coating used in this work had a thickness of less that 1 nm. The resulting GAIN medium (Figure 2b) is then ground to a powder and sonicated to create a GAIN suspension. Vacuum filtration of this suspension through the target waveguide directly embeds the GAIN fibers within it and creates a porous GAIN solid (Figure 2c). The resulting solid takes the geometry of the waveguide in which it is formed and can be mechanically removed if desired (Figure 2d). Direct integration in this manner allows for the target waveguide to be incorporated in a complete terahertz waveguide system. The integration method developed here is applicable to waveguides of arbitrary geometry, enabling more complex structures to be realized if desired. The lower cut-off frequency of the absorber and its impedance can be controlled via the cross-sectional dimensions of the target waveguide. Multiple absorbers can be created in parallel by using a target which contains multiple waveguides which are later separated through other means. In addition, this method can also be used to realize similarly arbitrary GAIN solids, which may be of interest in other applications.

Two integrated GAIN absorbers were realized using the above procedure, each of thickness 0.84 mm. These are denoted Sample 1 and Sample 2 in the remainder of this work. The samples were characterized using visual inspection, Raman spectroscopy, X-ray photoelectron spectroscopy (XPS), and electromagnetic measurements. SEM images of the absorbers were taken at varying magnification levels to allow examination of the GAIN solid's macro- and micro-structure (**Figure 3**a,b). Both samples fill the waveguide in a uniform manner, showing the efficacy of the integration method used here. The surface morphology of each sample is largely similar, although the front side of Sample 2 is smoother than that of Sample 1 (Figure 3a). Examination of Sample 2 under high magnification (Figure 3b) reveals that the GAIN solid is comprised of clusters of nanofibers separated by air pockets of size less than 1 μm. The fibers are randomly oriented, as opposed to their aligned orientation in the source GAIN material (Figure 2b).

The characteristic G peak at 1585 cm^{-1} and the symmetric 2D peak at 2675 cm^{-1} observed in the Raman spectra of the samples (Figure 3c) indicate the presence of mono- to few-layered graphene. The high intensity D peak at 1335 cm^{-1} indicates the presence of polycrystaline graphene with a high degree of disorder (with an intensity ratio I_D/I_G = 2.36 and 2.45 for the two samples, determined by decomposing the spectra with fitted peaks). Two additional defect-induced peaks D' (overlapping with the G peak) and D + D' at 2915 cm^{-1} are observed, which are also attributed to the presence of graphene flakes covering the rough surface of the nanofibers, as was previously shown by transmission electron microscopy in.[41] The XPS spectrum of Sample 2 (Figure 3d) also illustrates the presence of the graphene coating as a thin layer and the expected alumina oxide peaks. The combined Raman and XPS spectra confirm that the integration method outlined above (grinding, sonication, and vacuum filtration) did not chemically modify the GAIN structure as compared to the original material.[28] As such, we conclude that the sample preparation leads to a re-orientation and clustering of the fibers alone, as evidenced by the SEM images of the samples.

Electromagnetic characterization of the samples was performed from 67 to 500 GHz using the wideband waveguide measurement setup detailed in Section 4.3. This setup allows for measurement of the S-parameters of a single absorber sample across the entire frequency range, eliminating the need for multiple samples. The target waveguide cassette is designed to be above cutoff at the lowest frequency of operation (67 GHz), where the fundamental TE_{10} mode operates. The measurement bandwidth extends far beyond the cutoff frequency of the first higher mode (TE_{20}); the target waveguide thus supports many higher order modes which will propagate within the sample if excited. A chain of waveguide tapers is used to ensure that these higher order modes are not excited and ensure single-mode TE_{10} propagation at all frequencies. Additional time gating was applied to remove the effect of reflections caused by misalignment between the tapers, frequency extender, and waveguide cassette assembly. The measured S-parameters of the embedded GAIN samples (**Figure 4**) show that the material offers excellent absorption of electromagnetic energy across a wide band of frequencies. The measured insertion loss between

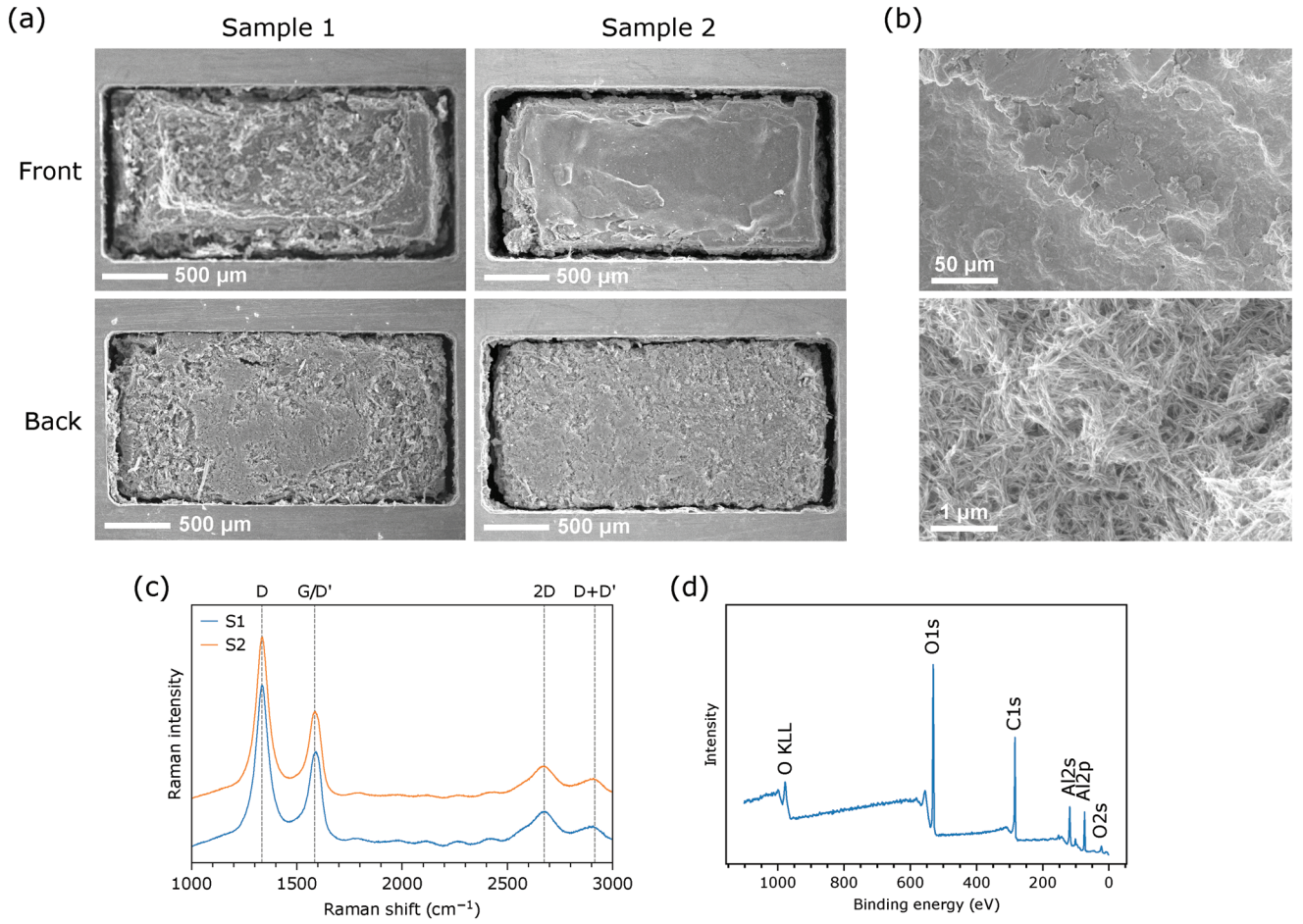

Figure 3. a) SEM images of the front and back sides of the samples inside the waveguide. b) High magnification SEM of the GAIN nanostructure. c) Raman spectra of the two samples (S1, S2) measured with a 532 nm laser. d) XPS survey spectrum of Sample 2.

67 and 110 GHz is greater than 20 dB and exceeds 40 dB at frequencies above 400 GHz. The reflection coefficient of the GAIN samples below 200 GHz is in excess of –10 dB, indicating that much of the incident energy is reflected by the step change in impedance at the material's interface at these frequencies. The short electrical length of the samples at these frequencies ($0.2\lambda_0$ at 88.5 GHz) leads to a relatively low insertion loss, despite the material's high reflectivity. The air gap between the GAIN material and the sidewalls of the metallic waveguide causes a slight increase in the impedance of the structure, as its effective width is reduced. Above 200 GHz, the GAIN samples exhibit a reflection coefficient below –10 dB. This value exceeds –20 dB for Sample 1 at frequencies above 450 GHz, showing that the material is well-matched to the empty waveguide. The measured reflection coefficient and insertion loss of empty reference waveguide of equivalent length to the absorber samples are also plotted in Figure 4. Although time gating was applied to all data, the effect of higher-order modes and resonances caused by the experimental setup is still evident in the measured reflection coefficient of the reference waveguides. The high loss of the GAIN material effectively dampens any such resonances and as such they are not observed in the corresponding measured data. The measured reflection loss of the GAIN samples exceeds that reported in ref. [13] showing the promise of this material for wideband terahertz systems and applications. The qualified absorption bandwidth of the GAIN absorbers (defined by frequencies where reflection loss is greater than 10 dB) exceeds 200 GHz. The monotonic behavior of the material indicates that the absorption bandwidth reported here is limited by the measurable frequency range, not the performance of the material itself.

The attenuation per unit-length of the two samples and a linear regression of the measured data are plotted in **Figure 5**a. The attenuation per unit length of the two samples exceeds 35 dB mm^{-1} for frequencies above 200 GHz and is as high as 50 dB mm^{-1} (35 dB/λ_0) at 500 GHz. The attenuation of both samples follows a linear trend across all measurement bands, increasing monotonically. The rate of increase in attenuation is similar for both samples (0.056 and 0.06 dB GHz^{-1}, for Samples 1 and 2, respectively). Sample 1 has a higher level of attenuation across all measured frequencies. The attenuation of Sample 2 increases sharply between 200 and 230 GHz. It is not clear whether this behavior is due to a frequency dependent characteristic of Sample 2 (such as internal resonances within the material) or if it is a measurement artefact. The similarity of the resonances observed for both Sample 1 and 2 at 480 GHz

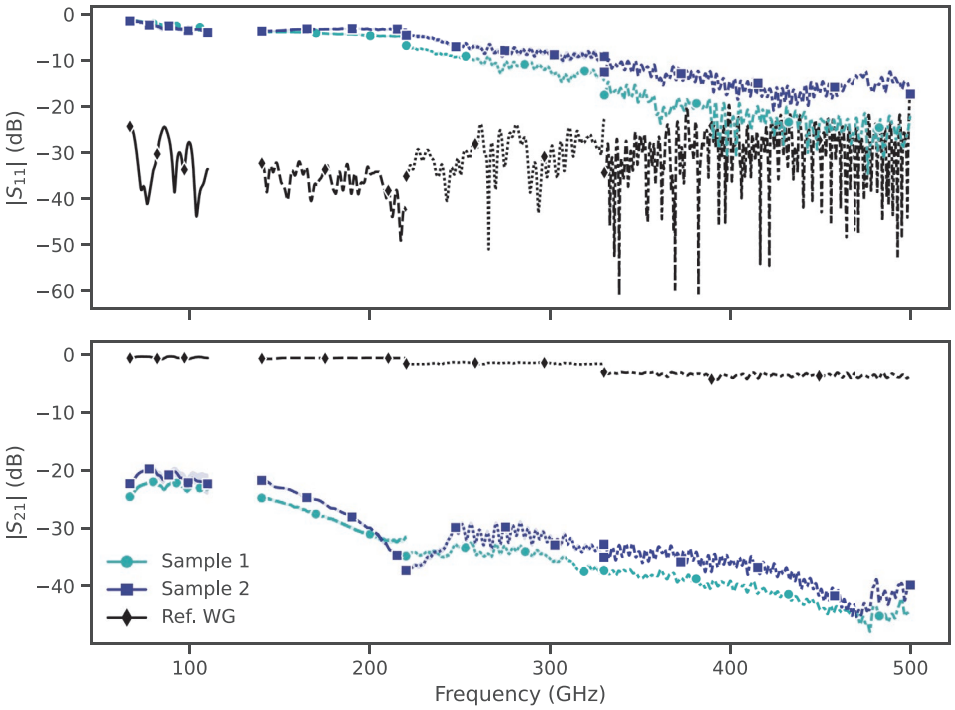

Figure 4. Measured $|S_{11}|$ and $|S_{21}|$ of the two waveguide embedded GAIN samples and the empty reference waveguide (Ref. WG) for each waveguide band post time gating.

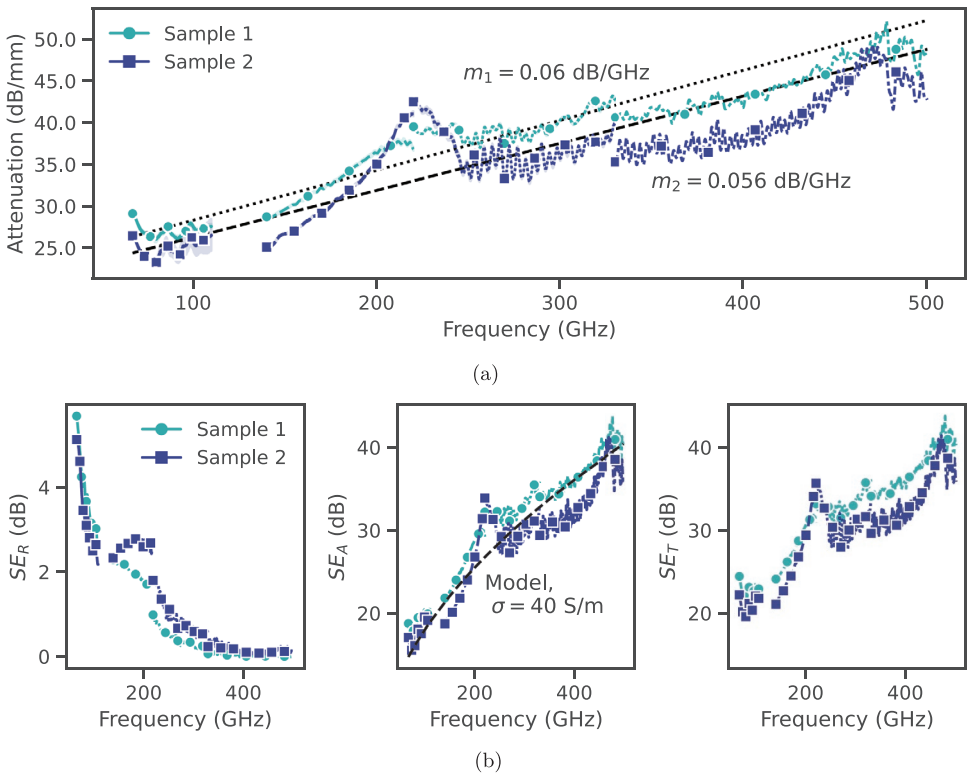

Figure 5. a) Normalized attenuation per unit length of the two embedded GAIN samples across all measured frequencies. The dashed lines represent a linear regression of the measured data for each sample, where each line has slope m. The 95% confidence intervals are represented by the shaded areas where available. b) Measured shielding effectiveness due to reflection (SE_R) and absorption (SE_A). The total effectiveness is given by SE_T. The SE_A was modeled using Equation (5) with an effective conductivity of $\sigma = 40$ S m^{-1}, where this value was obtained by curve fitting of the measured data. The modeled SE_A is represented by the dashed black trace.

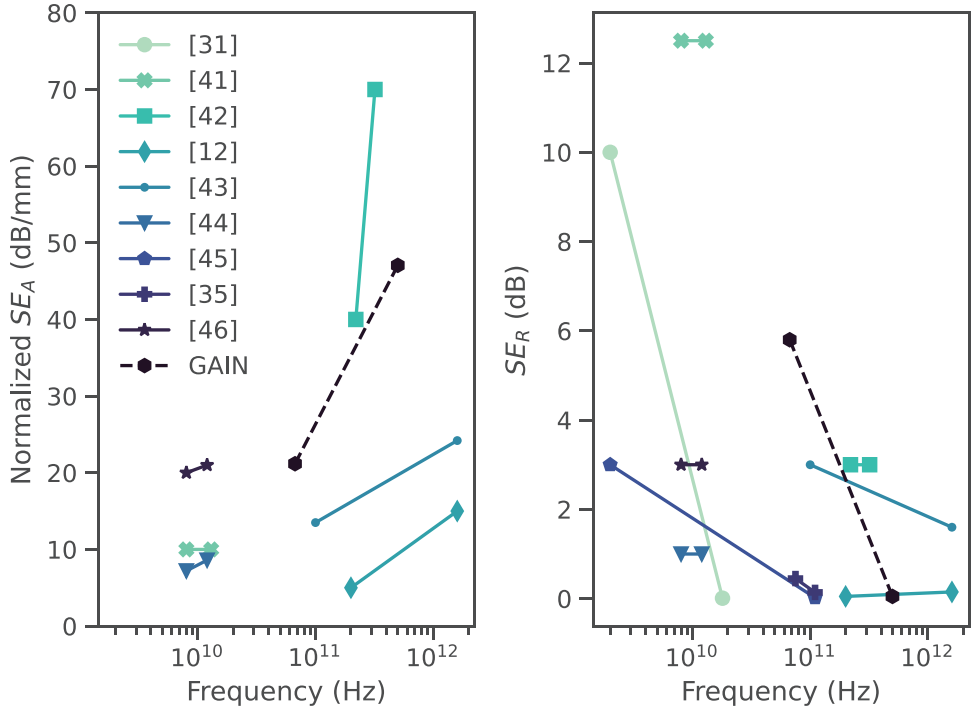

Figure 6. Comparison of SE_A and SE_R for graphene-based foam type absorbers reported in[12,31][35,41–46] and that reported here (GAIN) at the minimum and maximum measured frequency. The SE_A data has been normalized to the thickness of each material to allow a direct comparison. No SE_A was reported in ref. [45] or ref. [35].

indicates that these phenomena are measurement artefacts. Raman and XPS spectroscopy of both samples (Figure 3) found their chemical composition to be nearly identical. We conclude that the slight difference in observed behavior of the two samples is not related to their constitution. The difference in measured reflection coefficient and insertion loss may be due to the slight differences in sample geometry, waveguide filling factor and experimental uncertainty.

The shielding efficiency of the absorbers was determined from the measured S-parameter data. The shielding efficiency due to reflection (SE_R), absorption (SE_A) and the total shielding efficiency (SE_T) of both samples are plotted in Figure 5b. The theoretical shielding efficiency due to absorption (SE_A) was also modeled using Equation (5), where a conductivity of 40 S m^{-1} was found to provide an accurate fit to the measured data across all frequencies. This value was extracted via curve-fitting of the measured SE_A and is in good agreement with the DC conductivity ranges reported for GAIN in ref. [41] and represents the effective high-frequency conductivity of the absorber material at room temperature. The SE_T of both samples exceeds 20 dB at all frequencies, where absorption (SE_A) is seen to be the dominant shielding mechanism.

The total shielding efficiency of the GAIN samples presented here exceeds that of other potential terahertz absorber materials.[12,13,43,47] The shielding performance of the GAIN absorbers is compared to that of state-of-the-art graphene-based foam absorbers in **Figure 6**, where the reported SE_A has been normalized to the thickness of each material to allow for direct comparison. The GAIN absorbers reported here offer the highest normalized SE_A and lowest SE_R above 330 GHz of any such absorber published to date. In addition, the devices presented here are the first integrated terahertz waveguide absorbers yet reported. The performance of these devices is expected to be further improved at frequencies above 500 GHz, making them extremely promising for next generation integrated terahertz systems.

Despite their short electrical length both samples offer very high attenuation and low reflection coefficient. Neither sample exhibits the narrow-band response observed for many previously published graphene-based absorbers;[30] instead, they offer a smooth frequency response across the entire measurement band, making them well suited for wideband applications. The primary absorption mechanisms of the GAIN absorbers are graphically illustrated in **Figure 7**. Here, the incident wave (of power level P_i) impinges on an idealized GAIN solid comprised of randomly distributed nanofibers, resulting in a reflected wave (with power P_r) and transmitted wave (P_t). The power absorbed in the material, P_a, is defined as $P_i = P_r + P_a + P_t$. For an idealized absorber, the entire incident wave is attenuated in the material without generating a reflected wave (i.e., $P_r = P_t = 0$, $P_a = P_i$). Achieving $P_r = 0$ is not-feasible in practice, as the lossy nature of absorber materials creates a change in impedance at the material's interface which reflects part of the incident wave. However, the highly porous microstructure of the GAIN material allows electromagnetic waves to permeate into the material, leading to reduced reflectivity. At low frequencies, the features of the porous structure become electrically small and thus the GAIN samples act as a single effective medium, where its lossy nature creates a large interficial impedance change, causing the high reflectivity observed below

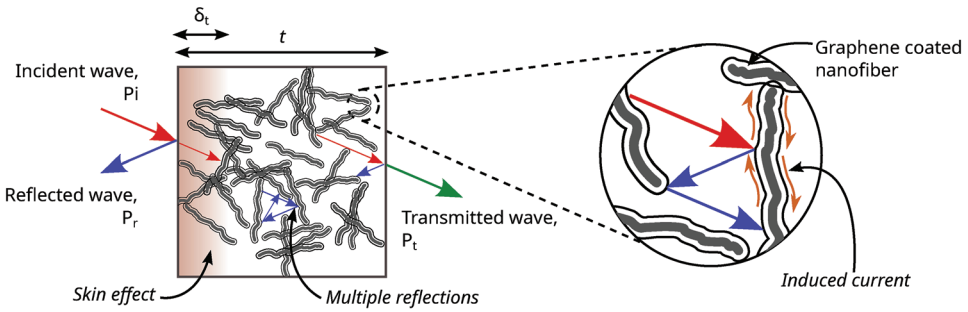

Figure 7. Schematic illustration of the absorption mechanisms of the integrated GAIN absorber.

200 GHz. This effect was also observed in ref. [41] where all measured samples displayed high reflectivity. The remaining incident signal penetrates into the material, where it induces currents in the GAIN fibers due to the presence of electric dipoles.[36] The conductivity of these fibers is due the presence of sp^2 carbon in their coating, which is an excellent conductor at high frequencies.[35] The skin effect[48] is a result of the conductive nature of the material, limiting the depth to which incident signals can penetrate. This phenomena causes significant absorption of the material, which is attenuated by a factor of $1/e$ at the skin-depth (δ_t). The skin depth of the GAIN absorbers developed here is between 0.3 and 0.1 mm (c.f. Equation (6)). As such, the experimental samples are between 2.8 and 8.4 skin depths thick, resulting in high attenuation to all incident waves. The tightly-bound nature of the nanofibers leads to multiple reflections and scattering within the material, as reported for other nanostructured absorbers.[43] These effects appear to play a minor role in the attenuation observed here—the theoretical value of SE_A (Figure 5b) provides an accurate fit to the measured RF and DC data without accounting for such higher-order effects. Electromagnetic absorbance was found to be the major contributor to shielding effectiveness at all frequencies. This is in contrast to other materials and is of great importance in terahertz system applications, where there are often strict requirements on reflected power levels.

The mechanical characteristics of the GAIN absorbers were not studied in this work. Further studies are required to properly quantify GAIN's mechanical properties. Depending on the chosen application the robustness of the absorber material may be critical to the long-term performance of the device. In systems applications, the GAIN material would not undergo additional manipulation post integration, negating the risk for destruction of the material. The adhesion of the GAIN to the metallic waveguide could be improved to eliminate the air gaps seen in Figure 3 and prevent potential displacement of the material. In addition, the thermal behavior of this material should be examined prior to its use in systems applications to ensure that the impedance of the material is stable across the expected operating temperature range. The lossy nature of the material leads to localized joule heating within the absorber, which could potentially cause thermal damage if the incident energy was sufficiently high. Dielectric breakdown within the material could also occur in such a scenario. The breakdown power level of air for the waveguide used here is between 16 and 20 kW from 100 and 500 GHz (Equation (7)), which is further increased by the dielectric nature of the GAIN material. The graphene coating was deposited at temperatures around 1000 °C. Due to the limited power levels available at such frequencies we do not consider thermal or breakdown damage to be a relevant risk.

3. Conclusion

This article presented a simple method to directly integrate terahertz absorbers based on graphene-augmented inorganic nanofibers in waveguide systems and analyzed their electromagnetic performance from 67 to 500 GHz. These absorbers offer excellent absorption across the entire measured frequency band as well as low reflectivity for frequencies above 200 GHz, with an attenuation per unit length of up to 50 dB mm^{-1}. Low reflectivity is achieved despite the high absorbance due to the porous nature of the material following deposition in the waveguide. The qualified absorption bandwidth of the absorbers (>200 GHz) is limited by the measurable frequency range rather than the properties of the material itself. The integration method developed here does not require freeze-drying or other chemical treatment, in contrast to existing methods. This method may also be of interest for realizing GAIN solids comprised of randomly oriented nanofibers. In addition, the wideband waveguide measurement setup proposed in this work is applicable to the study of many other kinds of materials and eliminates the need to prepare multiple samples. The GAIN absorber material is a very promising candidate for high frequency integrated waveguide systems and applications due to its outstanding electromagnetic properties. Unlike many existing alternatives, the material proposed here can be scaled to higher frequencies, modified to arbitrary cross-sectional geometries and integrated in a complete system without additional complexity.

4. Experimental Section

Sample Preparation: A gamma-alumina nanofiber sample with average fiber diameter of 10 nm and length of 2 cm was located in a hot-wall chemical vapor deposition (CVD) reactor for realization of the GAIN material. These fibers were chosen to provide effective absorbtion across all frequencies of interest and due to the stability of their fabrication process. Carbon coating was deposited from methane at a temperature of 1000 °C, with a dwell time of 10 min, following the procedure previously reported elsewhere.[28] The resulting coating consisted of a few layers of polycrystalline graphene which was wrapped around the alumina nanofibers. The proportion of deposited carbon was 10–13 wt% for the samples reported here.

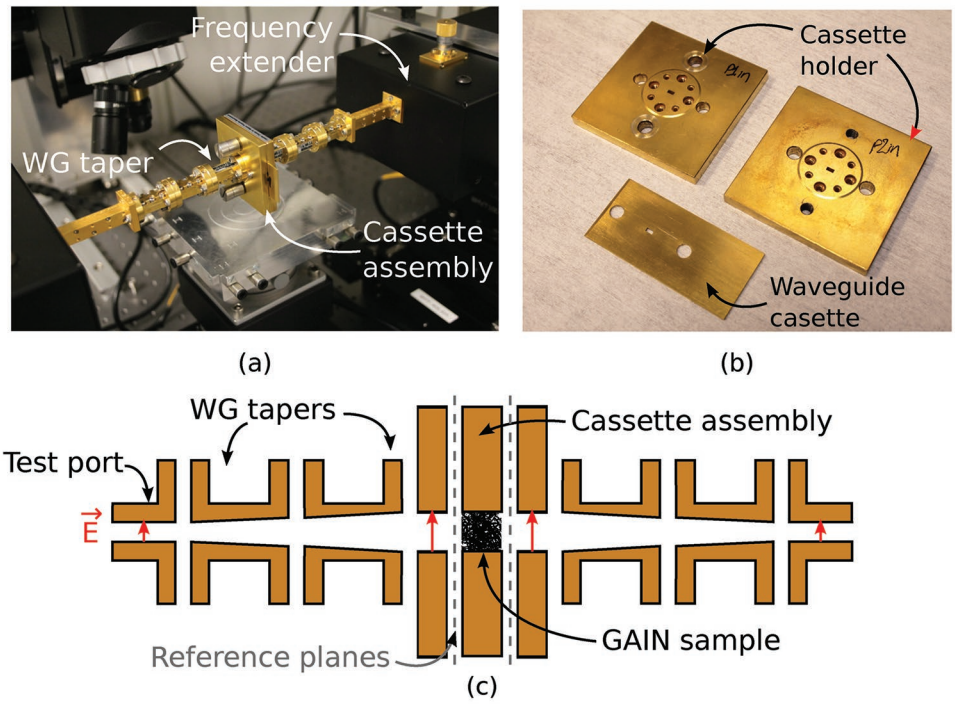

Figure 8. a) Test setup used for RF characterization, wherein the cassette assembly of (b) is connected to the relevant frequency extenders using a chain of waveguide tapers. b) Waveguide cassette assembly (Elmika Ltd., Vilnius, Lithuania). c) Schematic drawing of the test setup. The reference planes for all measured data are also indicated.

To embed the GAIN material in the waveguide cassette, it was initially ground in a mortar and then sonicated in ethanol for 20 min using an ultrasonic processor (Hielscher UP400S, input power 20 W). Vacuum filtration (Millipore) was used to deposit the material inside a hollow rectangular waveguide cassette, which was later connected to a specialized sample holder for RF characterization of the material (Section 4.3). Mechanical removal of the excess material was carefully performed to ensure the GAIN material was constrained to the waveguide cassette. The waveguide cassette used here was 0.84 mm long and had cross-sectional dimensions of 2.54 mm × 1.27 mm.

Compositional Characterization: Scanning electron microscopy (SEM) images of the waveguide embedded GAIN were acquired with a Zeiss Ultra 55 SEM between 5 and 30 kV with an in-lens SE detector. A complete analysis of the microstructure of GAIN samples prepared using the methods described here can be found in ref. [41].

Raman spectra of the samples were acquired with a Horiba LabRAM HR 800 system with a 532 nm (2.33 eV, 5.6 mW) Nd:YAG laser, 600 l mm^{-1} grating, 50 × (0.42 NA) objective, 2 s exposure time, and 100 accumulations.

XPS was performed with a Physical Electronics Quantera II Scanning XPS Microprobe with an Al Kα monochromatic X-ray source (1486.6 eV) and 100 µm beam diameter. The survey spectrum between 0 and 1100 eV was recorded with a 0.8 eV resolution.

Electromagnetic Characterization: To characterize its electromagnetic behavior, the GAIN material was connected to a vector network analyzer (VNA, Rohde & Schwarz ZVA-24), allowing the S-parameters of the waveguide embedded material to be measured. Commercial VNA frequency extender units were used to up-convert the operational frequency of the VNA to THz frequencies. The operation of these extenders was restricted to four discrete measurement bands – from 67 to 110 GHz (Agilent N5260A), 140–220 GHz (Rohde & Schwarz ZC220), 220–330 GHz (Rohde & Schwarz ZC330) and 330 and 500 GHz (Virginia Diodes Inc. WM570-VNAX). As previously described, the GAIN material was embedded inside a hollow rectangular waveguide of cross-sectional dimension 2.54 mm × 1.27 mm. This waveguide had a nominal operational frequency band of 67–110GHz (Wr-10), which was determined by the cut-off frequencies of its fundamental T_{10} mode and the higher-order TE_{20} mode. In order to analyze the RF performance of the samples at frequencies above 110 GHz a set of linear waveguide tapers (Elmika Ltd., Vilnius, Lithuania) is used to allow connection of the Wr-10 waveguide cassette to rectangular waveguides of smaller cross-section (**Figure 8**a). These tapers were inserted between the sample and the test ports of the corresponding frequency extender. They provided a smooth impedance transition between the two different waveguides and restricted the generation of higher-order waveguide modes in the test setup. Single-mode propagation in the material at all frequencies was thus assumed. The discontinuities observed between the various measurement bands were due to the use of different frequency extender units at each band. A special cassette holder (Elmika Ltd., Vilnius, Lithuania) was used to allow the material to be inserted in a standard THz waveguide test setup. This holder consisted of two gold-coated brass plates between which the cassette is mounted (Figure 8b). The plates were fastened together using a set of springs and screw fixings. The complete assembly was then inserted between the waveguide tapers for the given measurement frequency band. An empty waveguide cassette of equivalent length to the sample was used to provide reference data for each of the above measurement bands. Measurements of the GAIN samples were performed sequentially starting from 67 GHz. Each sample was measured multiple times and was removed and replaced in the cassette holder between measurements. The resulting standard deviation of the measured data provided an indication of the level of experimental uncertainty. Mechanical degradation of the GAIN samples occurred during the removal/replacement process. As such, only one measurement of each sample could be performed between 330 and 500GHz.

A through-reflect-line calibration[49] was performed at each measurement band using a waveguide calibration kit to correct systematic measurement errors associated with the vector network analyzer and frequency extenders. This process shifts the reference plane of the measurement up to the waveguide test ports of each frequency

extender. Any misalignment between the taper(s) and waveguide test ports or sample cassette led to the generation of higher-order modes and standing waves in the measurement setup. These effects inhibited the accurate measurement of the sample material. Time gating could be used to correct such effects[50] and was applied to all measured data. A time gate of length 0.8–1 ns was first applied to the measurement of the empty reference waveguides, wherein the correct location for the gate was determined from the time domain response of the empty waveguide. These settings were then used to apply time gating to each sample in a given measurement band. This procedure reduced high frequency variations in the measured data and dampened the response of any resonances caused by misalignment or other defects in the test setup. The normalized attenuation of the GAIN samples was determined by normalizing the measured data in each band to the insertion loss of the corresponding empty waveguide. This process removed any excess insertion loss caused by conductive losses in the waveguide tapers. Linear regression was performed using a first order least-squares fit to the mean response of the time gated data for each sample.

The shielding efficiency of the material was determined using the equations outlined in ref. [51]

$$A_{\text{eff}} = (1-|S_{11}|^2-|S_{21}|^2)/(1-|S_{11}|^2) \quad (1)$$

$$\text{SE}_R = -10\log_{10}(1-|S_{11}|^2)\,(\text{dB}) \quad (2)$$

$$\text{SE}_A = -10\log_{10}(1-A_{\text{eff}})\,(\text{dB}) \quad (3)$$

$$\text{SE}_T = \text{SE}_R + \text{SE}_A \quad (4)$$

where A_{eff}, SE_R and SE_A represent the effective absorbance and shielding efficiency due to reflection and absorption, respectively. SE_T is the total shielding effectiveness. The effect of multiple reflections (SE_M) had been neglected here as SE_A exceeds 15 dB for both samples.[52] Equations (1) and (3) allowed for the absorbance of the material to be assessed independent of the level of measured reflection coefficient. The normalized $|S_{21}|$ was used in all calculations to ensure that the excess insertion loss caused by the waveguide tapers did not affect the results. The standard Simon model for shielding efficiency[53] was used to model the theoretical SE_A of the absorbers via the equation

$$\text{SE}_A(\text{dB}) = 1.7(t/\rho)f^{\gamma} \quad (5)$$

where t is the sample thickness in cm, ρ its resistivity in Ω cm, f the frequency in MHz, and γ the frequency exponent. Standard curve fitting of the measured data was used to determine the effective conductivity ($\sigma = 1/\rho$) of the material (Figure 5b). A value of $\gamma = 0.5$ was used in all calculations. The skin depth of the material was determined using

$$\delta_t = \frac{1}{\sqrt{\pi f \mu \sigma}} \quad (6)$$

where f is the frequency of interest, μ the permeability of the sample, and σ its conductivity. A value of $\mu = \mu_0$ was used throughout.

The breakdown power level of a hollow rectangular waveguide is[54]

$$P_b = E_0 \frac{ab}{4}\left(\frac{\varepsilon_0}{\mu_0}\right)^{1/2}\left[1-\frac{\lambda_0}{2a}^2\right]^{1/2} \quad (7)$$

where E_0 is the incident electric field strength, a and b are the width and height of the waveguide, ϵ_0 and μ_0 free-space permittivity and permeability and λ_0 the free-space wavelength at the frequency of operation. Breakdown occurred in air at electric field strengths in excess of 30 kV cm^{-1}.

Acknowledgements

The authors acknowledge Myfab for provisioning of facilities and experimental support. Myfab was funded by the Swedish Research Council as a national research infrastructure. The work was supported by the European Union's Horizon 2020 FET Open project TERAmeasure (grant agreement No 862788). The Estonian Research Foundation (ETAG) under the grant PRG643.

Conflict of Interest

The authors declare no conflict of interest.

Data Availability Statement

Research data are not shared.

Keywords

absorber, graphene, integration, nanofiber, shielding, terahertz, waveguide

Received: January 27, 2022
Revised: March 3, 2022
Published online: April 7, 2022

[1] P. H. Siegel, *IEEE Trans. Microwave Theory Techn.* **2002**, *50*, 910.
[2] K. Sengupta, T. Nagatsuma, D. M. Mittleman, *Nat. Electron.* **2018**, *1*, 622.
[3] S. S. Dhillon, M. S. Vitiello, E. H. Linfield, A. G. Davies, M. C. Hoffmann, J. Booske, C. Paoloni, M. Gensch, P. Weightman, G. P. Williams, E. Castro-Camus, D. R. S. Cumming, F. Simoens, I. Escorcia-Carranza, J. Grant, S. Lucyszyn, M. Kuwata-Gonokami, K. Konishi, M. Koch, C. A. Schmuttenmaer, T. L. Cocker, R. Huber, A. G. Markelz, Z. D. Taylor, V. P. Wallace, J. Axel Zeitler, J. Sibik, T. M. Korter, B. Ellison, S. Rea, et al., *J. Phys. D: Appl. Phys.* **2017**, *50*, 043001.
[4] H. Elayan, O. Amin, B. Shihada, R. M. Shubair, M.-S. Alouini, *IEEE Open J. Commun. Soc.* **2020**, *1*, 1.
[5] S. Dang, O. Amin, B. Shihada, M.-S. Alouini, *Nat. Electron.* **2020**, *3*, 20.
[6] E. C. Strinati, S. Barbarossa, J. L. Gonzalez-Jimenez, D. Ktenas, N. Cassiau, L. Maret, C. Dehos, *IEEE Vehicular Tech. Mag.* **2019**, *14*, 42.
[7] H. Sarieddeen, N. Saeed, T. Y. Al-Naffouri, M. Alouini, *IEEE Commun. Mag.* **2020**, *58*, 69.
[8] D. M. Mittleman, *Opt. Express* **2018**, *26*, 9417.
[9] J. C. Pearson, B. J. Drouin, S. Yu, *IEEE J. Microwaves* **2021**, *1*, 43.
[10] H. Matsumoto, I. Watanabe, A. Kasamatsu, Y. Monnai, *Nat. Electron.* **2020**, *3*, 122.
[11] X. Fu, F. Yang, C. Liu, X. Wu, T. J. Cui, *Adv. Opt. Mater.* **2020**, *8*, 1900628.
[12] S.-T. Xu, F. Fan, J. Cheng, H. Chen, W. Ma, Y. Huang, S. Chang, *Adv. Opt. Mater.* **2019**, *7*, 1900555.
[13] H. Chen, W. Ma, Z. Huang, Y. Zhang, Y. Huang, Y. Chen, *Adv. Opt. Mater.* **2018**, *7*, 1801318.
[14] J. Campion, A. Hassona, Z. S. He, B. Beuerle, A. Gomez-Torrent, U. Shah, S. Vecchiattini, R. Lindman, T. S. Dahl, Y. Li, H. Zirath, J. Oberhammer, *IEEE Trans. Terahertz Sci. Technol.* **2019**, *9*, 624.
[15] H. Hubers, *IEEE J. Sel. Top. Quantum Electron.* **2008**, *14*, 378.
[16] E. J. Wollack, D. J. Fixsen, A. Kogut, M. Limon, P. Mirel, J. Singal, *IEEE Trans. Instrum. Meas.* **2007**, *56*, 2073.
[17] J. W. Kooi, R. A. Reeves, A. W. Lichtenberger, T. J. Reck, A. K. Fung, S. Weinreb, J. W. Lamb, R. S. Gawande, K. A. Cleary, G. Chattopadhyay, *IEEE Trans. Terahertz Sci. Technol.* **2018**, *8*, 434.

[18] S. Venkatachalam, K. Zeranska-Chudek, M. Zdrojek, D. Hourlier, *Nano Select* **2020**, *1*, 471.
[19] T. Ellam, in *Proc. of IEEE Symp. on Electromagnetic Compatibility*, IEEE, Piscataway, NJ **1994**, p. 408.
[20] B.-X. Wang, Y. He, P. Lou, W. Xing, *Nanoscale Adv.* **2020**, *2*, 763.
[21] X. Cheng, R. Huang, J. Xu, X. Xu, *ACS Appl. Mater. Interfaces* **2020**, *12*, 33352.
[22] A. S. Saadeldin, M. F. O. Hameed, E. M. A. Elkaramany, S. S. A. Obayya, *IEEE Sens. J.* **2019**, *19*, 7993.
[23] J. Huang, J. Li, Y. Yang, J. Li, J. Li, Y. Zhang, J. Yao, *Opt. Express* **2020**, *28*, 17832.
[24] H. Yang, D. Chen, Y. Mao, J. Yang, *Nanomaterials* **2020**, *10*, 1844.
[25] Y. Qing, W. Zhou, F. Luo, D. Zhu, *Carbon* **2010**, *48*, 4074.
[26] C. Méjean, L. Pometcu, R. Benzerga, A. Sharaiha, C. Le Paven-Thivet, M. Badard, P. Pouliguen, *Mater. Sci. Eng.: B* **2017**, *220*, 59.
[27] Z. Lin, J. Liu, W. Peng, Y. Zhu, Y. Zhao, K. Jiang, M. Peng, Y. Tan, *ACS Nano* **2020**, *14*, 2109.
[28] I. Hussainova, R. Ivanov, S. N. Stamatin, I. V. Anoshkin, E. M. Skou, A. G. Nasibulin, *Carbon* **2015**, *88*, 157.
[29] Q. Song, F. Ye, L. Kong, Q. Shen, L. Han, L. Feng, G. Yu, Y. Pan, H. Li, *Adv. Funct. Mater.* **2020**, *30*, 31 2000475.
[30] Q. Li, Z. Zhang, L. Qi, Q. Liao, Z. Kang, Y. Zhang, *Adv. Sci.* **2019**, *6*, 1801057.
[31] M. Qin, L. Zhang, X. Zhao, H. Wu, *Adv. Funct. Mater.* **2021**, *31*, 2103436.
[32] I. V. Anoshkin, A. G. Nasibulin, Y. Tian, B. Liu, H. Jiang, E. I. Kauppinen, *Carbon* **2014**, *78*, 130.
[33] I. Huynen, L. Bednarz, J.-M. Thomassin, C. Pagnoulle, R. Jerome, C. Detrembleur, in *2008 38th European Microwave Conf.*, IEEE, Piscataway, NJ **2008**, p. 5.
[34] N. Quiévy, P. Bollen, J.-M. Thomassin, C. Detrembleur, T. Pardoen, C. Bailly, I. Huynen, *IEEE Trans. Electromagn. Compat.* **2012**, *54*, 43.
[35] I. V. Anoshkin, J. Campion, D. V. Lioubtchenko, J. Oberhammer, *ACS Appl. Mater. Interfaces* **2018**, *10*, 19806.
[36] M. Biabanifard, M. S. Abrishamian, *Appl. Phys. A* **2018**, *124*, 826.
[37] E. Zareian-Jahromi, M. Nourbakhsh, R. Basiri, V. Mashayekhi, *Appl. Opt.* **2021**, *60*, 7297.
[38] M. M. Ghods, P. Rezaei, *J. Electromagn. Waves Appl.* **2018**, *32*, 1950.
[39] Y. Wu, N. Yi, L. Huang, T. Zhang, S. Fang, H. Chang, N. Li, J. Oh, J. A. Lee, M. Kozlov, A. C. Chipara, H. Terrones, P. Xiao, G. Long, Y. Huang, F. Zhang, L. Zhang, X. Lepró, C. Haines, M. D. Lima, N. P. Lopez, L. P. Rajukumar, A. L. Elias, S. Feng, S. J. Kim, N. T. Narayanan, P. M. Ajayan, M. Terrones, A. Aliev, P. Chu, et al., *Nat. Commun.* **2015**, *6*, 6141.
[40] R. Shu, G. Zhang, C. Zhang, Y. Wu, J. Zhang, *Adv. Electron. Mater.* **2021**, *7*, 2001001.
[41] A. S. Shamshirgar, R. E. Rojas Hernández, G. C. Tewari, J. F. Fernández, R. Ivanov, M. Karppinen, I. Hussainova, *ACS Appl. Mater. Interfaces* **2021**, *13*, 21613.
[42] Z. Barani, F. Kargar, K. Godziszewski, A. Rehman, Y. Yashchyshyn, S. Rumyantsev, G. Cywiński, W. Knap, A. A. Balandin, *ACS Appl. Mater. Interfaces* **2020**, *12*, 28635.
[43] Z. Huang, H. Chen, S. Xu, L. Y. Chen, Y. Huang, Z. Ge, W. Ma, J. Liang, F. Fan, S. Chang, Y. Chen, *Adv. Opt. Mater.* **2018**, *6*, 1801165.
[44] Y. Yuan, L. Liu, M. Yang, T. Zhang, F. Xu, Z. Lin, Y. Ding, C. Wang, J. Li, W. Yin, Q. Peng, X. He, Y. Li, *Carbon* **2017**, *123*, 223.
[45] Y. Zhang, Y. Huang, T. Zhang, H. Chang, P. Xiao, H. Chen, Z. Huang, Y. Chen, *Adv. Mater.* **2015**, *27*, 2049.
[46] Z. Chen, C. Xu, C. Ma, W. Ren, H.-M. Cheng, *Adv. Mater.* **2013**, *25*, 1296.
[47] D. Polley, A. Barman, R. K. Mitra, *Optics Lett.* **2014**, *39*, 1541.
[48] M. W. Jaroszewski, S. Thomas, A. V. Rane, (Eds.) *Advanced materials for electromagnetic shielding: fundamentals, properties, and applications*, Wiley, Hoboken, NJ **2019**, 1.
[49] G. Engen, C. Hoer, *IEEE Trans. Microwave Theory Tech.* **1979**, *27*, 12.
[50] D. Ma, X. Shang, N. M. Ridler, W. Wu, *IEEE Trans. Instrum. Meas.* **2021**, *70*, 6005904.
[51] Y. K. Hong, C. Y. Lee, C. K. Jeong, D. E. Lee, K. Kim, J. Joo, *Rev. Sci. Instrum.* **2003**, *74*, 1098.
[52] J. Joo, A. J. Epstein, *Appl. Phys. Lett.* **1994**, *65*, 2278.
[53] R. M. Simon, *Polym.-Plast. Technol. Eng.* **1981**, *17*, 1.
[54] P. Lorrain, D. R. Corson, F. Lorrain, *Electromagnetic Fields and Waves: Including Electric Circuits*, 3rd ed. Freeman, Newyork **1988**, p. 754.